Research Article | Vol. 24, No. 24 | 28 Nov 2016 | OPTICS EXPRESS 27494

Optics EXPRESS

DM/LCWFC based adaptive optics system for large aperture telescopes imaging from visible to infrared waveband

FEI SUN,[1,2] ZHAOLIANG CAO,[1,*] YUKUN WANG,[1,2] CAIHUA ZHANG,[1,2] XINGYUN ZHANG,[1] YONG LIU,[1,2] QUANQUAN MU,[1] AND LI XUAN[1]

[1]*State Key Lab of Applied Optics, Changchun Institute of Optics, Fine Mechanics and Physics, Chinese Academy of Sciences, Changchun, Jilin, 130033, China*
[2]*University of Chinese Academy of Sciences, Beijing, 100049, China*
[*]*caozlok@ciomp.ac.cn*

Abstract: Almost all the deformable mirror (DM) based adaptive optics systems (AOSs) used on large aperture telescopes work at the infrared waveband due to the limitation of the number of actuators. To extend the imaging waveband to the visible, we propose a DM and Liquid crystal wavefront corrector (DM/LCWFC) combination AOS. The LCWFC is used to correct the high frequency aberration corresponding to the visible waveband and the aberrations of the infrared are corrected by the DM. The calculated results show that, to a 10 m telescope, DM/LCWFC AOS which contains a 1538 actuators DM and a 404 × 404 pixels LCWFC is equivalent to a DM based AOS with 4057 actuators. It indicates that the DM/LCWFC AOS is possible to work from visible to infrared for larger aperture telescopes. The simulations and laboratory experiment are performed for a 2 m telescope. The experimental results show that, after correction, near diffraction limited resolution USAF target images are obtained at the wavebands of 0.7-0.9 μm, 0.9-1.5 μm and 1.5-1.7 μm respectively. Therefore, the DM/LCWFC AOS may be used to extend imaging waveband of larger aperture telescope to the visible. It is very appropriate for the observation of spatial objects and the scientific research in astronomy.

OCIS codes: (010.1080) Active or adaptive optics; (090.1000) Aberration compensation; (230.3720) Liquid-crystal devices.

References and links

1. G. Herriot, S. Morris, A. Anthony, D. Derdall, D. Duncan, J. Dunn, A. Ebbers, J. M. Fletcher, T. Hardy, B. Leckie, A. Mirza, C. Morbey, M. Pfleger, S. Roberts, P. Shott, M. Smith, L. Saddlemyer, J. Sebesta, K. Szeto, B. Wooff, W. Windels, and J. P. Veran, "Progress on Altair: the Gemini North adaptive optics system," Proc. SPIE **4007**, 115–125 (2000).
2. G. Rousset, F. Lacombe, P. Puget, E. Gendron, R. Arsenault, P. Kern, D. Rabaud, P. Y. Madec, N. Hubin, G. Zins, E. Stadler, J. Charton, P. Gigan, and P. Feautrier, "Status of the VLT Nasmyth adaptive optics system (NAOS)," Proc. SPIE **4007**, 72–81 (2000).
3. H. Takami, S. Colley, M. Dinkins, M. Eldred, O. Guyon, T. Golota, M. Hattori, Y. Hayano, M. Ito, M. Iye, S. Oya, Y. Saito, and M. Watanabe, "Status of Subaru laser guide star AO system," Proc. SPIE **6272**, 62720C (2006).
4. C. E. Max, B. A. Macintosh, S. Gibbard, D. T. Gavel, H. G. Roe, I. de Pater, A. M. Ghez, D. S. Acton, P. L. Wizinowich, and O. Lai, "Neptune and Titan observed with Keck telescope adaptive optics," Proc. SPIE **4007**, 213–220 (2000).
5. F. Roddier, *Adaptive Optics in Astronomy* (Cambridge University, 1999) Chap. 1.
6. J. Roberts, A. H. Bouchez, R. S. Burruss, R. G. Dekany, S. R. Guiwits, and M. Troy, "Optical characterization of the PALM-3000 3388-actuator deformable mirror," Proc. SPIE **77362**, 77362 (2010).
7. J. E. Roberts, R. G. Dekany, R. S. Burruss, C. Baranec, A. Bouchez, E. E. Croner, S. R. Guiwits, D. D. S. Hale, J. R. Henning, D. L. Palmer, M. Troy, T. N. Truong, and J. Zolkower, "Results from the PALM-3000 high-order adaptive optics system," Proc. SPIE **8447**, 84470Y (2012).
8. J. M. Booth, "Adaptive optical microscopy: the ongoing quest for a perfect image," Light Sci. Appl. **3**(4), e165 (2014).
9. S. R. Restaino, D. M. Payne, J. T. Baker, J. R. Andrews, S. W. Teare, G. C. Gilbreath, D. Dayton, and J. Gonglewski, "Liquid crystal technology for adaptive optics: un update," Proc. SPIE **5003**, 187–192 (2003).

#276491 http://dx.doi.org/10.1364/OE.24.027494
Journal © 2016 Received 26 Sep 2016; revised 29 Oct 2016; accepted 9 Nov 2016; published 17 Nov 2016

Optics EXPRESS

10. K. A. Bauchert, S. A. Serati, and A. Furman, "Advances in liquid crystal spatial light modulators," Proc. SPIE **4734**, 35–43 (2002).
11. Z. Cao, Q. Mu, H. Xu, P. Zhang, L. Yao, and L. Xuan, "Open loop liquid crystal adaptive optics systems: progresses and results," Proc. SPIE **9676**, 1–7 (2015).
12. Q. Mu, Z. Cao, D. Li, L. Hu, and L. Xuan, "Open-loop correction of horizontal turbulence: system design and result," Appl. Opt. **47**(23), 4297–4301 (2008).
13. H. Chen, L. Xuan, L. Hu, Z. Cao, and Q. Mu, "Design of open-loop liquid crystal adaptive optical system for 1200 mm telescope," Opt. Precision Eng. **18**(1), 29–36 (2010).
14. Q. Mu, Z. Cao, L. Hu, Y. Liu, Z. Peng, and L. Xuan, "Novel spectral range expansion method for liquid crystal adaptive optics," Opt. Express **18**(21), 21687–21696 (2010).
15. Z. Cao, Q. Mu, L. Hu, Y. Liu, Z. Peng, Q. Yang, H. Meng, L. Yao, and L. Xuan, "Optimal energy-splitting method for an open-loop liquid crystal adaptive optics system," Opt. Express **20**(17), 19331–19342 (2012).
16. Z. Peng, Y. Liu, L. Yao, Z. Cao, Q. Mu, L. Hu, and L. Xuan, "Improvement of the switching frequency of a liquid-crystal spatial light modulator with optimal cell gap," Opt. Lett. **36**(18), 3608–3610 (2011).
17. Z.-H. Peng, Y.-G. Liu, L.-S. Yao, Z.-L. Cao, Q.-Q. Mu, L.-F. Hu, X.-H. Lu, L. Xuan, and Z.-Y. Zhang, "Improvement of response performance of liquid crystal optical devices by using a low viscosity component," Chin. Phys. Lett. **28**(9), 0942071 (2011).
18. H. Hu, L. Hu, Z. Peng, Q. Mu, X. Zhang, C. Liu, and L. Xuan, "Advanced single-frame overdriving for liquid-crystal spatial light modulators," Opt. Lett. **37**(16), 3324–3326 (2012).
19. Z. Peng, Y. Liu, Z. Cao, Q. Mu, L. Yao, L. Hu, C. Yang, R. Wu, and L. Xuan, "Fast response property of low-viscosity difluorooxymethylene-bridged liquid crystals," Liq. Cryst. **40**(1), 91–96 (2013).
20. D. Dayton, J. Gonglewski, S. Restaino, J. Martin, J. Phillips, M. Hartman, P. Kervin, J. Snodgress, S. Browne, N. Heimann, M. Shilko, R. Pohle, B. Carrion, C. Smith, and D. Thiel, "Demonstration of new technology MEMS and liquid crystal adaptive optics on bright astronomical objects and satellites," Opt. Express **10**(25), 1508–1519 (2002).
21. Q. Mu, Z. Cao, L. Hu, Y. Liu, Z. Peng, L. Yao, and L. Xuan, "Open loop adaptive optics testbed on 2.16 meter telescope with liquid crystal corrector," Opt. Commun. **285**(6), 896–899 (2012).
22. Z. Cao, Q. Mu, L. Hu, D. Li, Y. Liu, L. Jin, and L. Xuan, "Correction of horizontal turbulence with nematic liquid crystal wavefront corrector," Opt. Express **16**(10), 7006–7013 (2008).
23. Z. Cao, Q. Mu, L. Hu, X. Lu, and L. Xuan, "A simple method for evaluating the wavefront compensation error of diffractive liquid-crystal wavefront correctors," Opt. Express **17**(20), 17715–17722 (2009).
24. R. Conan, C. Bradley, P. Hampton, O. Keskin, A. Hilton, and C. Blain, "Distributed modal command for a two-deformable-mirror adaptive optics system," Appl. Opt. **46**(20), 4329–4340 (2007).
25. X. Lin, Y. Liu, L. Wang, G. Wang, and F. Wei, "Performance test and experiment of correction capability of 137-element deformable mirror," Opt. Precision Eng. **21**(2), 267–273 (2013).
26. Q. Mu, Z. Cao, Z. Peng, Y. Liu, L. Hu, X. Lu, and L. Xuan, "Modal interaction matrix measurement for liquid-crystal corrector: precision evaluation," Opt. Express **17**(11), 9330–9336 (2009).
27. R. J. Noll, "Zernike polynomials and atmospheric turbulence," J. Opt. Soc. Am. **66**(3), 207 (1976).
28. J. W. Hardy, *Adaptive Optics for Astronomical Telescope* (Oxford University, 1998).
29. Z. Cao, L. Xuan, L. Hu, Y. Liu, and Q. Mu, "Effects of the space-bandwidth product on the liquid-crystal kinoform," Opt. Express **13**(14), 5186–5191 (2005).
30. D. Dayton, S. Browne, and J. Gonglewski, "Increasing the bandwidth of a liquid crystal phased array adaptive optics system," Proc. SPIE **5894**, 58940M (2005).

1. Introduction

Adaptive optics systems (AOSs) have been widely used on ground based large aperture telescopes, such as Gemini, VLT, Subaru and Keck etc, to overcome the effects of the atmospheric turbulence [1–4]. In all of these AOSs, the deformable mirrors (DMs) are used to correct the aberration caused by the atmospheric turbulence and the number of actuator is inversely proportional to the atmospheric turbulence coherence length r_0. As the r_0 is proportional to the relevant wavelength, the number of actuator corresponding to the visible waveband is more than that of the infrared [5]. The actuator number of the DM is restricted by the fabrication technology and the maximum is 3388 up to now [6]. Furthermore, the AOSs are restricted by the wavefront sensor with corresponding higher resolution and the computational requirements of the control algorithm. To avoid these problems, most of the AOSs used on large aperture telescopes are operated in the infrared waveband at present. However, the visible waveband is very important for the observation of spatial objects and the scientific research in astronomy. To realize this, dual DMs based AOS PALM-3000 has been manufactured and used on 5.1 m Hale Telescope [7]. It contains two DMs which have 241 and 3388 actuators respectively. Although this AOS can correct the distortions for the visible waveband, it is very complicated and then, very difficult to be realized. Furthermore, the

Optics EXPRESS

telescope with aperture more than 5.1 m still cannot be operated in the visible waveband with adaptive correction.

Liquid crystal wavefront correctors (LCWFCs) have been widely investigated as they have the advantages of high spatial resolution, easy fabrication, low cost, and compact size [8–10], LCWFC is very appropriate to be used onto larger aperture telescope to realize high accuracy correction because it has thousands upon thousands pixels. However, it has the shortcomings of slow response and low energy efficiency. As the LCWFC has the polarization dependence and chromatism, its optical efficiency is very low. To solve these problems, a novel optical system design is performed based on an open loop control method [11–13]. In this novel optical system, the incoming light is firstly split into two beams with a dichroic beam splitter: the beam with the waveband of 0.4-0.7 μm is used to detect the distortion; the other with the waveband of 0.7-0.9 μm is corrected by the LCWFC and then, goes to the imaging camera. To avoid the polarization energy loss, the light with the waveband of 0.7-0.9 μm is split into two linear polarized beams by a polarized beam splitter (PBS) and each beam is corrected with its corresponding LCWFC. After correction, the two beams are combined into one beam again and then, imaged by a camera [14, 15]. As the correction error and the energy loss of the LCWFC are acceptable at the narrow waveband of 0.7-0.9 μm, the energy efficiency of the LC AOS is greatly improved and it is very closed to that of the DM based AOS. Moreover, the response speed of the LCWFC is improved greatly by designing and synthesizing the novel liquid crystal materials [16, 17], and applying the overdriving technique [18]. Now, the response time of the LCWFC has been down to sub-millisecond [11, 19], and this is comparable to that of the DMs. Consequently, the liquid crystal adaptive optics system (LC AOS) may be used to correct the atmospheric turbulence for large aperture telescope and it has been tested on different telescopes [20–22]. However, because of the dispersion of liquid crystal materials, the LCWFC can only work at a narrow waveband 0.7-0.9 μm [15].

From above we can see that, the DM has the advantage of wide working waveband (from visible to infrared) and the disadvantage of low spatial resolution; but the LCWFC has the advantage of high spatial resolution and the disadvantage of narrow working waveband (0.7-0.9 μm). If the advantages of the DM and LCWFC can be combined, the disadvantages of them can be avoided felicitously. Therefore, in this paper, we expect to combine the DM and LCWFC to obtain an AOS which can work from visible to infrared waveband for larger aperture telescopes.

2. Principle and configuration

To expand the working waveband of the DM based AOS to the visible band, a DM/LCWFC combination AOS is considered. To correct the distortions of the ground based telescope produced by the atmospheric turbulence, the required actuator number of the DM can be approximately calculated as:

$$N = (D / r_0)^2. \tag{1}$$

Where D is the diameter of the telescope aperture and r_0 is the coherence length of atmospheric turbulence.

Because r_0 increases as the 6/5 power of the wavelength [5], the actuator number of DM will be drastically decreased while the relevant wavelength becomes longer according to Eq. (1). For example, to a 10 m telescope and r_0 = 10 cm, assuming the working wavelength is 0.8 μm and 1.6 μm, the required actuator number of DM is 4057 and 772 respectively. Therefore, the DM is very suitable for the correction of the turbulence at the infrared but not the visible waveband for larger aperture telescope. However, the LCWFC is very applicable to working at the visible waveband because of its high spatial resolution. Consequently, it is expected to expand the working waveband to the visible with the DM/LCWFC combination AOS.

Optics EXPRESS

Normally, the atmospheric dispersion can be approximately ignored in the astronomical adaptive optics. Based on this assumption, we expect that the DM can correct the aberration of the infrared and the residual is corrected by the LCWFC. Thus, all the aberrations can be removed and the high resolution images can be obtained from visible to infrared waveband. The schematic diagram of a DM/LCWFC combination AOS is shown in Fig. 1. The distorted wavefront of the target light is compensated by the DM firstly, and then is split into two beams with dichroic filter 1: the light of long waveband is imaged by an infrared camera; the other with the waveband of 0.4-0.9 μm is split again with the dichroic filter 2. The reflected light with the waveband of 0.4-0.7 μm goes into the Shack-Hartmann wavefront sensor (S-H WFS) to detect the aberrations; the transmitted beam with waveband of 0.7-0.9 μm is corrected further by the LCWFC and then, imaged by a visible camera. To this configuration, the DM can be controlled with closed-loop method as the S-H WFS follows the DM. However, as the S-H WFS is blind to the LCWFC, it can only be operated with open-loop control.

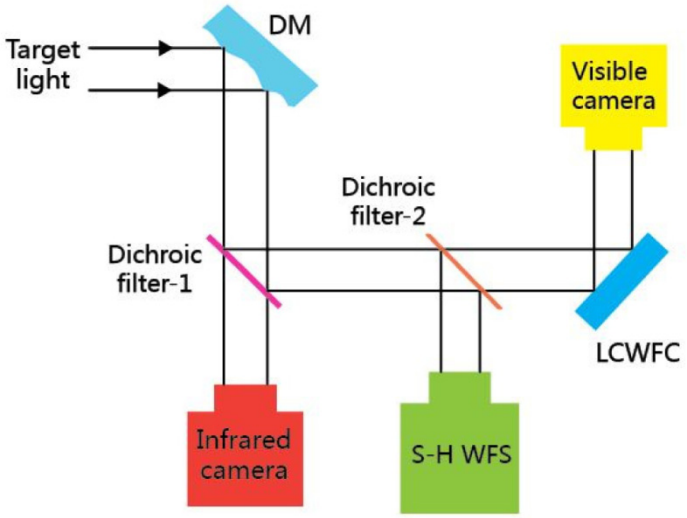

Fig. 1. Schematic diagram of the DM/LCWFC combination AOS

To illustrate the advantages of the DM/LCWFC combination AOS, the relation between the actuators and the aperture of the telescope is analyzed. The visible and infrared waveband of 0.7-0.9 μm and 1.1-1.3 μm are selected respectively to do the analysis. The atmospheric turbulence coherence length r_0 equals to 10 cm (at the wavelength of 0.55 μm). To do the comparison, the number of the actuator is also calculated for DM based AOS according to Eq. (1). For the DM based AOS, the actuators must match with the short waveband (0.7-0.9 μm), and r_0 equals to 15.7 cm. To the DM/LCWFC combination AOS, as the LCWFC is utilized to correct the aberrations of the short waveband, the actuators of the DM only needs to match with the long waveband (1.1-1.3 μm) and then, r_0 equals to 25.5 cm. Thus, the required actuators of the DM may be calculated for the DM and DM/LCWFC based AOSs according to Eq. (1) and the calculated results are shown in Fig. 2(a). It indicated that, compared to the DM based AOS, the number of actuators is decreased drastically for the DM/LCWFC based AOS. For example, to a 10 m telescope, the numbers of actuators are 4057 and 1538 respectively for the DM and DM/LCWFC based AOSs. Moreover, the required pixel number of the LCWFC is also computed with following equation [23]:

$$\langle P_N \rangle = 6.25Q + (15 - 1.5D - 23Q + 0.91QD) r_0^{-6/5}. \quad (2)$$

Optics EXPRESS

Where Q is the quantization level, D is the diameter of the telescope aperture, and the total pixel number of LCWFC is $P_N \times P_N$. Commonly, $Q = 8$ is suitable for atmospheric turbulence correction and the detailed information can be seen in [23], Z. Cao et al…. Figure 2(b) shows the relationship between the required pixel number P_N and the telescope aperture D. It is shown that the pixel number of the LCWFC is only 404 × 404 for 10 m telescope.

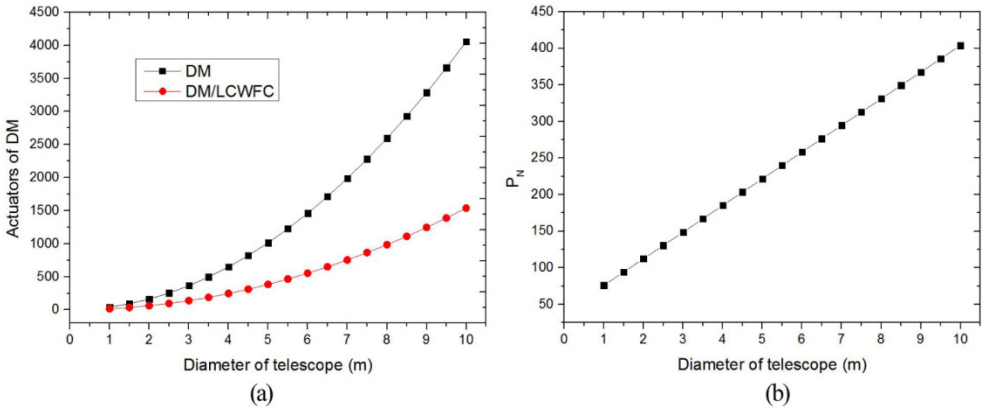

Fig. 2. Numbers of actuators as a function of the telescope aperture: (a) DM and DM/LCWFC; (b) LCWFC.

From the above calculation we can see that, for a 10 m telescope, the DM/LCWFC combination system only needs a DM with 1538 actuators and a LCWFC with 404 × 404 pixels and the working waveband will be extended to the visible. However, if only use a DM to correct the distortions from visible to infrared waveband, the actuators are 4057. Up to now, the maximum number of the actuator of the DM is 3388. Hence, the DM based AOS is almost impossible to correct the distortions of the visible waveband for larger aperture telescope, but it can be easily realized by using the DM/LCWFC system. With this optimal design, the advantages of the DM and LCWFC are well used and the astronomical high resolution observation is feasible in the visible waveband.

3. Numerical simulation

3.1 Assignment of the aberrations

To illustrate the validity of the DM/LCWFC AOS, a numerical simulation is performed. Normally, the DM and the LCWFC are controlled with the slopes acquired by the S-H WFS. In the paper, to simulate the aberration decomposition conveniently, Zernike polynomial is used to express the aberrations [24]. Therefore, the measured slopes should be transformed to the coefficients of Zernike polynomial to simulate the correction of the aberrations. The aberrations caused by the atmospheric turbulence may be expressed as:

$$\phi=\sum_{n=1}^{\infty} a_n Z_n=\sum_{n=1}^{m} a_n Z_n+\sum_{n=m+1}^{l} a_n Z_n+\varepsilon, \tag{3}$$

where Z_n is the n^{th} Zernike polynomial and a_n is the corresponding coefficient, ε is the residual error. To describe the aberration conveniently, $\phi_1=\sum_{n=1}^{m} a_n Z_n$ and $\phi_2=\sum_{n=m+1}^{l} a_n Z_n$ are defined and they are corrected by the DM and LCWFC respectively.

As ϕ_1 is corrected by the DM, it may be rewritten as:

Optics EXPRESS

$$\phi_1 = \sum_{i=1}^{k} v_i R_i(x, y), \tag{4}$$

where k is the actuator number, v_i represents the driving voltage and $R_i(x, y)$ is the interaction matrix of the i^{th} actuator. The interaction matrix of the DM may be measured by a ZYGO interferometer [25] and it can be described by the Zernike polynomial:

$$R_i(x, y) = \sum_{n=1}^{m} a_{in} Z_n. \tag{5}$$

Substituting Eq. (5) and $\phi_1 = \sum_{n=1}^{m} a_n Z_n$ into Eq. (4), the equation can be obtained as:

$$\sum_{n=1}^{m} a_n Z_n = \sum_{i=1}^{k} \sum_{n=1}^{m} v_i a_{in} Z_n. \tag{6}$$

By removing Z_n, Eq. (6) can be rewritten with the matrix form:

$$A_1 = V \cdot A_r, \tag{7}$$

where V is a the driving voltage matrix, A_1 is the measured aberration matrix, and A_r is the interaction matrix. Equation (7) can be rewritten as:

$$V = A_1 \cdot (A_r)^{-1}, \tag{8}$$

here $(A_r)^{-1}$ is the pseudo-inverse matrix of A_r. It indicates that the driving voltage can be calculated with the interaction matrix and the measured aberrations.

To the LCWFC, the interaction matrix is measured with Zernike polynomial method [26] and it may be expressed as:

$$M = C_1 \cdot A^{-1}, \tag{9}$$

where C_1 is the coefficient sent to the LCWFC, A is the responded coefficient measured by the S-H WFS and A^{-1} is the pseudo-inverse matrix of A.

To correct the aberrations of the atmospheric turbulence with the LCWFC, the reconstructed coefficient can be calculated as:

$$C_2 = M^{-1} \cdot A_2, \tag{10}$$

where M^{-1} is the pseudo-inverse matrix of M, A_2 is the coefficient of the aberrations and it can be measured by the S-H WFS. Thus, the correction signal may be acquired with the reconstructed coefficient C_2. To the DM/LCWFC AOS, the aberration ϕ_2 will be corrected by the LCWFC. Therefore, the Zernike modes of the measured coefficient A_2 is from $m + 1$ to l.

It can be seen that, assuming the interaction matrix of the DM and LCWFC is known and the atmospheric turbulence is produced, the correction of the aberration can be simulated with Eq. (8) and (10).

3.2 Simulation of the aberration correction

To simulate the correction of the atmospheric turbulence, an aberration caused by the atmospheric turbulence should be produced firstly. The atmospheric turbulence is produced with Noll's method [27]. A 2 m telescope and r_0 = 10 cm (at the wavelength of 785 nm) are used to perform the simulation. As the turbulence is mild, the intensity variation is ignored and we only consider the phase variation here. The first 77 modes of Zernike polynomial are used to produce the distorted wavefront caused by the atmospheric turbulence and one

Optics EXPRESS

hundred atmospheric turbulence wavefronts are used to obtain statistical results. Figure 3(a) shows the first 77 Zernike coefficients of the one hundred wavefronts and a representative wavefront is shown in Fig. 3(b). The tip/tilt aberrations are removed from the wavefront because they are corrected by a tip/tilt mirror (TTM). The peak to valley (PV) and root mean square (RMS) of the wavefront aberration are 3.46 μm and 0.68 μm respectively.

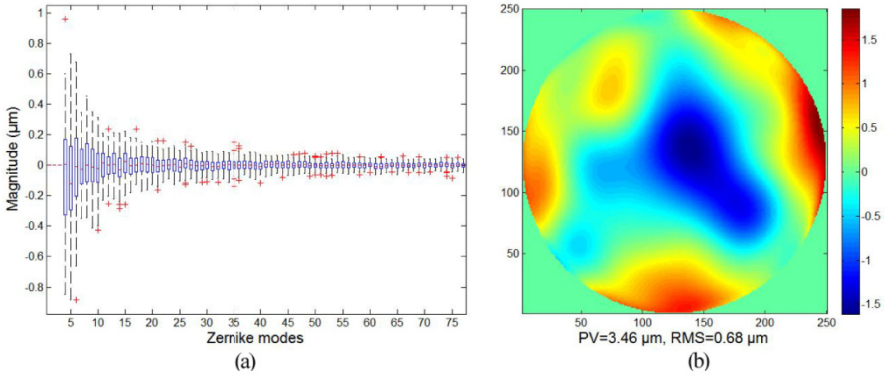

Fig. 3. Simulated atmospheric turbulence: (a) Coefficients of Zernike modes; (b) Wavefront

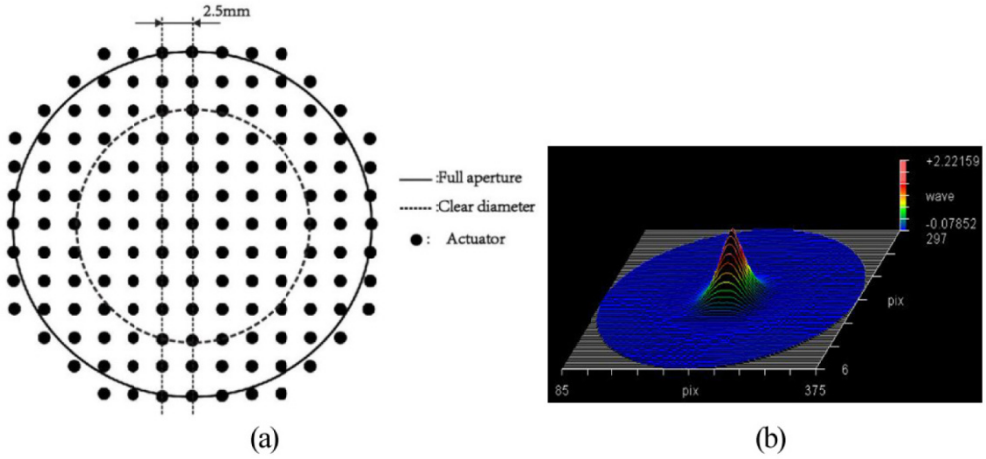

Fig. 4. Performance of the DM: (a) Configuration of the actuator; (b) Response of an actuator measured by ZYGO interferometer

While the atmospheric turbulence is corrected with the first J modes of Zernike polynomial, the residual can be calculated with [27]:

$$\sigma_{\varphi}^{2} \approx 0.294 J^{-\frac{\sqrt{3}}{2}} (\frac{D}{r_0})^{\frac{5}{3}}, \tag{11}$$

where J is the number of the Zernike modes. Normally, the residual less than 1 rad is acceptable for the applications of astronomy [28]. To the wavelength of 0.8 μm and 1.2 μm, the r_0 are 10.2 cm and 16.6 cm respectively and then the corresponding Zernike modes are 77 and 29 to obtain the residual of 1 rad. According to the assignment of the aberration, the first 29 Zernike modes are corrected by the DM and the 30-77 Zernike modes are corrected by the LCWFC.

Optics EXPRESS

To simulate the aberration correction of the DM, a DM (ALPAO) is selected with the parameters of 145 actuators, 30 mm aperture, and the resonance frequency of 4 kHz. The actuator configuration of the DM is shown in Fig. 4(a). We only use the central 97 actuators to do the correction and the clear aperture is 20 mm. The interaction matrix of the DM is measured with a ZYGO interferometer and the response of one actuator is shown in Fig. 4(b).

As the interaction matrix of the DM is measured and the distortions caused by the atmospheric turbulence may be calculated with Noll's method, the correction signal of the aberrations ϕ_1 can be computed with Eq. (8). The difference between the correction signal and the aberration ϕ is the correction error. One hundred atmospheric turbulence wavefronts are produced and corrected to obtain the statistical results. Figure 5(a) shows the Zernike coefficients after the correction of DM. It indicates that the first 29 Zernike modes are perfectly corrected and the residual of ϕ is about 0.12 μm. As an example, Fig. 5(b) shows one of the reconstructed wavefront with the interaction matrix of DM. by subtracting the reconstructed wavefront from the aberration wavefront shown in Fig. 3(b), the residual wavefront is shown in Fig. 5(c) with the PV of 0.95 μm and RMS of 0.12 μm respectively.

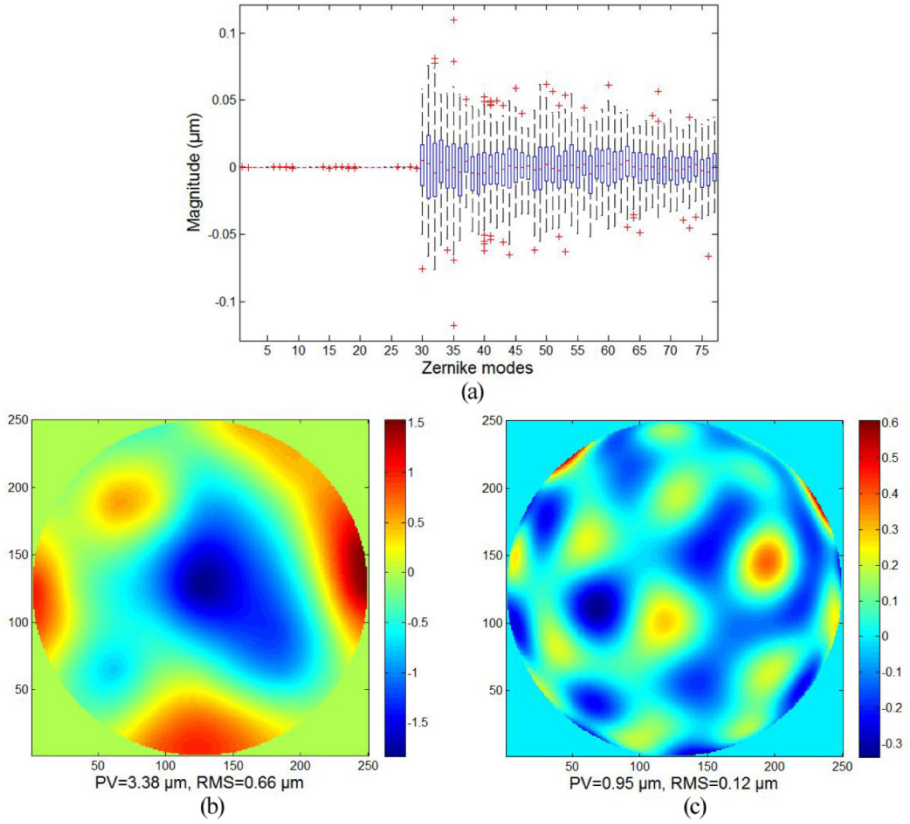

Fig. 5. Simulation of the wavefront correction by the DM: (a) Zernike coefficients of the residual wavefront; (b) Reconstructed wavefront; (c) Residual wavefront

After the correction of DM, the aberration ϕ_2 which contains the Zernike modes of 30-77 will be corrected with the LCWFC. Normally, the LCWFC utilizes the phase-wrapping technique to extend the magnitude of the phase modulation [29]. To realize the large phase modulation, the wavefront will be operated with modulo of 2π and then, quantified according to the pixel size of the LCWFC. Figure 6 shows the phase wrapping process of a tilt

Optics EXPRESS

aberration with the magnitude of 6π. The phase is firstly compressed into 2 π (Fig. 6(a)) and then, quantified as shown in Fig. 6(b). As the phase wrapping technique is used, the correction accuracy and the diffraction efficiency are sensitive to the wavelength. The results of the simulated analysis show that, for the waveband of 0.7-0.9 μm, the diffraction efficiency is decreased 3% and phase modulation error is about 1/10 λ [22, 29]. Therefore, assuming the minor energy loss and correction error is permitted, the LCWFC may be used to correct the aberrations for a narrow waveband.

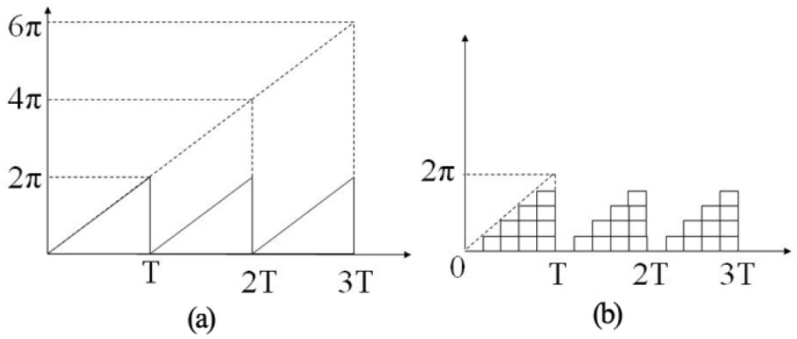

Fig. 6. Illustration of the phase wrapping: (a) Modulo of 2π; (b) Quantization

As the phase wrapping technique is used, the phase modulation of 1λ is required for the LCWFC. One LCWFC (BNS, P256) is used to do the simulation, which has 256 × 256 pixels and the array size of 5.8 × 5.8 mm. The response time of the LCWFC is measured and the response curve is shown in Fig. 7. It can be seen that the response time of the LCWFC is 0.75 ms when the modulation is 1 λ (λ = 785 nm). As the LCWFC has the correction frequency of 1.3 kHz, it is comparable to that of the DMs and then, the atmospheric turbulence may be corrected rapidly by the LCWFC.

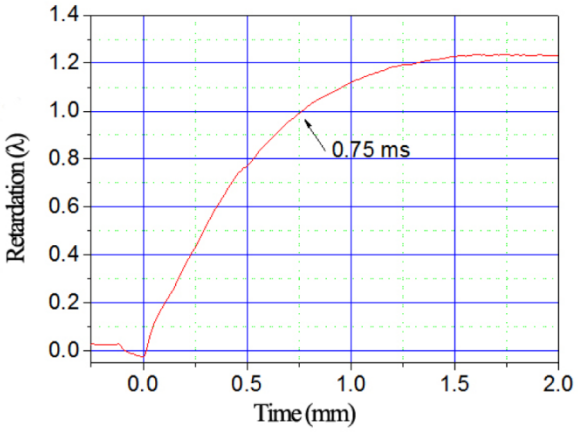

Fig. 7. Response curve of the LCWFC

The interaction matrix of the LCWFC is measured with the Zernike polynomial method [26]. Concretely, the different Zernike modes are sent to the LCWFC in turn and an S-H WFS is used to measure the response of each Zernike mode. The measured data is placed into a matrix which is called interaction matrix. A S-H WFS contains 20 × 20 microlenses and the frame rate of 2.7 kHz is selected to measure the interaction matrix of the LCWFC. As the response of 77 Zernike modes needs to be measured, the 20 × 20 microlenses is sufficient to do this.

Optics EXPRESS

The correction of the LCWFC can be simulated with the interaction matrix of the LCWFC. The simulation method for the LCWFC is similar to that of the DM and a hundred atmospheric turbulence wavefronts ϕ_2 are produced and corrected too. After correction of the DM and the LCWFC, the Zernike coefficients of Fig. 3(a) are decreased as shown in Fig. 8(a). It indicates that the first 77 Zernike modes are perfectly corrected with the dual correctors of DM and LCWFC. The simulated results show that, the average residual of ϕ is about 0.03 μm after correction. As an example, the residual wavefront (Fig. 5(c)) is corrected further by the LCWFC. Figure 8(b) shows the reconstructed wavefront with the interaction matrix of LCWFC and the corrected wavefront is shown in Fig. 8(c) with PV of 0.44 μm and RMS of 0.02 μm respectively. The simulated results indicate that the DM/LCWFC combination AOS may be used to correct the atmospheric turbulence.

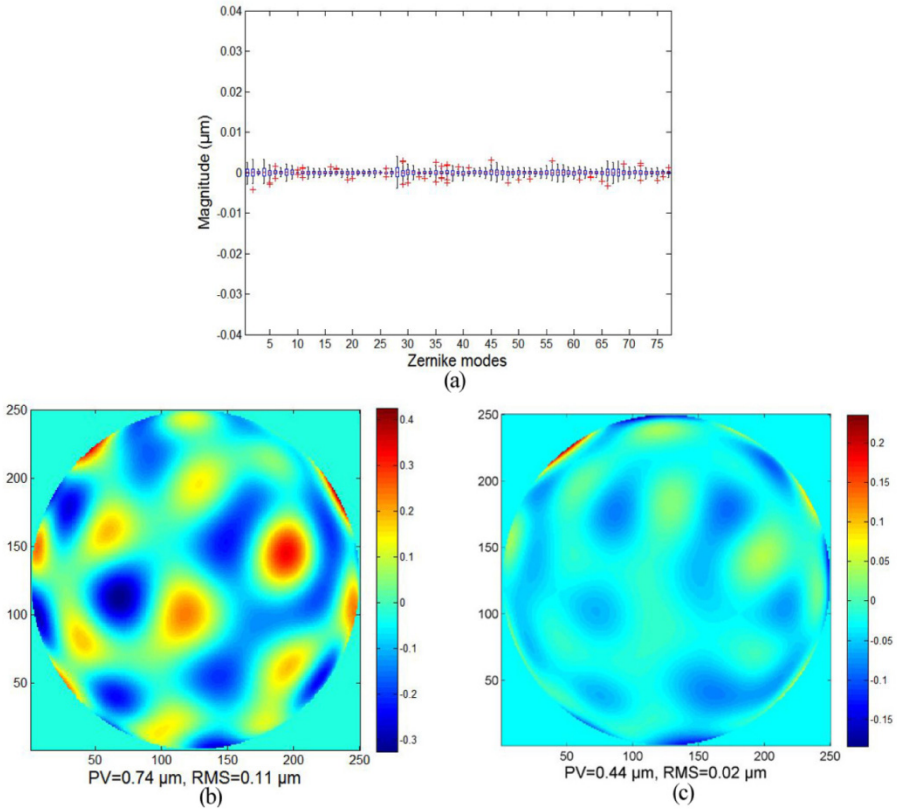

Fig. 8. Simulation of the wavefront correction by the LCWFC and DM: (a) Zernike coefficients of the residual wavefront; (b) Reconstructed wavefront; (c) Residual wavefront

4. Experiment

To evaluate the validity of the DM/LCWFC AOS, some optical devices are chosen for the AOS. A Xenon lamp is selected as the light source with the spectrum range of 0.4-1.7 μm. The tip-tilt mirror (TTM) has 25 mm aperture, ± 2 mrad magnitude, and resonance frequency of 2.6 kHz. The DM, LCWFC and S-H WFS used in the experiment have been presented in the simulation section. An atmospheric turbulence simulator is used to generate the distortions and atmospheric turbulence coherence length is about 1mm at the wavelength of 785 nm. The aperture of the atmospheric turbulence simulator is 100 mm. The phase screen can be rotated by a variable speed stepping motor and the Greenwood frequency can be generated from 0 Hz to more than 200 Hz. To simulate the atmospheric turbulence for a 2 m

Optics EXPRESS

telescope with r_0 = 10 cm, the sub-aperture of 20 mm is selected on the phase screen of the atmospheric turbulence. As only one phase screen is used, the effect of the propagation is not considered here.

Based on the selected devices, the optical setup of the DM/LCWFC AOS is shown in Fig. 9. The light emitted from the fiber is collimated by an achromatic lens and then reflected by the DM. To simplify the light path, the phase screen is located after the DM as it has no effect on the correction experiment. Then the beam is reflected by the TTM. The reflected light is split into two beams by the long wave pass filter 1 (LWPF1) with a split point of 0.9 μm: one is transmitted and then focused on the infrared camera; the reflected light is zoomed out with a pair of lens and then, goes to the LWPF2 with a split point of 0.7 μm. The incident light is split by the LWPF2 into two beams: one is reflected and goes into the S-H WFS for the aberration detection; the transmitted light goes to the LCWFC and then, is reflected and imaged by a visible CCD camera, a PBS is placed before the LCWFC to produce polarized light. Furthermore, the infrared waveband 0.9-1.7 μm is split into 0.9-1.5 μm and 1.5-1.7 μm respectively with the LWPF3. With this optical design, the waveband of 0.4-0.7 μm is used for wavefront detection and the imaging wavebands are 0.7-0.9 μm, 0.9-1.5 μm and 1.5-1.7 μm respectively.

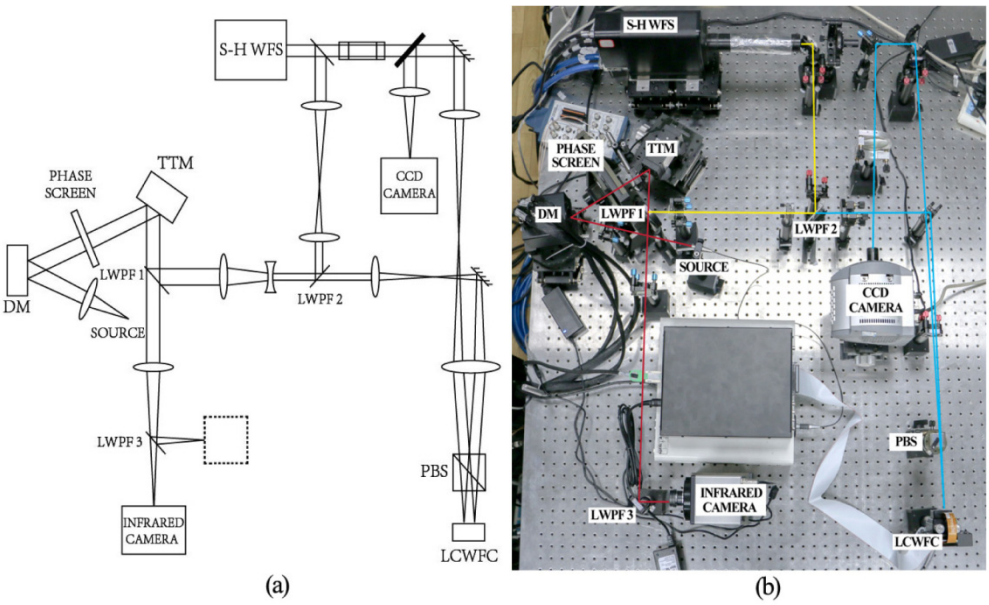

Fig. 9. Optical layout of the DM/LCWFC AOS: (a) Designed; (b) Experimental configuration

Firstly, the system bandwidth of the LCWFC is measured. The disturbance rejection bandwidth is defined as [30]:

$$rej(dB) = 20\log_{10}(\frac{OutputDisturbanceAmplitude}{InputDisturbanceAmplitude}). \quad (12)$$

Therefore, the disturbance and the residual must be measured to obtain the system bandwidth. As the LCWFC is controlled with open loop method, the S-H WFS cannot measure the residual. Consequently, the CCD camera is replaced with another S-H WFS to measure the correction error of the LCWFC. The TTM is used to produce different frequency sinusoidal tilt aberrations and they will be corrected by the LCWFC. The input tilt amplitude is measured, and then with the correction of the LCWFC, the output tilt amplitude can be measured too. The disturbance rejection ability of the LCWFC is measured as shown in Fig.

Optics EXPRESS

10. It can be seen that the −3dB rejection frequency of the LCWFC is about 80 Hz which is comparable to that of the DM.

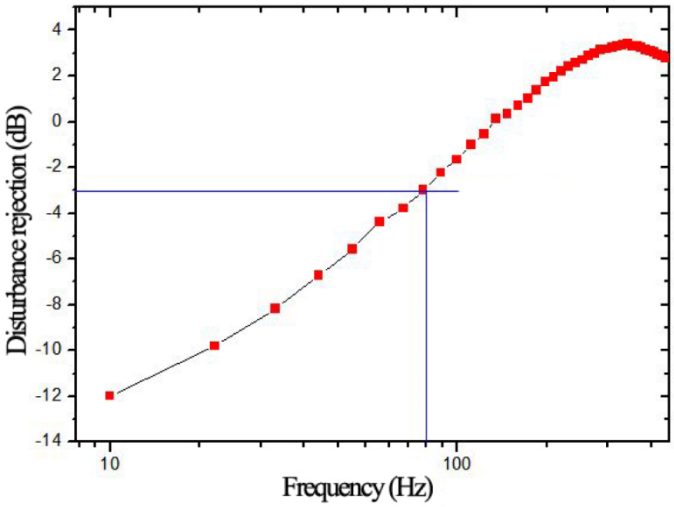

Fig. 10. Disturbance rejection as a function of tilt frequency

To the DM/LCWFC AOS, the DM and the LCWFC are operated with closed-loop control and open-loop control [11, 12] methods respectively. To compare with the simulated results, the first 29 and 30-77 Zernike modes are corrected by the DM and LCWFC respectively. As the aperture of the beam is 20 mm, 97 actuators of the DM are used to perform the aberration correction. The distortions are produced by the atmospheric turbulence simulator and the phase screen is rotated with the velocity of 118.5 mm/s to produce with the Greenwood frequency of 50 Hz. While the adaptive correction is started, the DM and LCWFC correct the distortions simultaneously.

Before correction, a static distortion is measured as shown in Fig. 11(a) with PV = 4.43 μm and RMS = 0.61 μm. After correction, the residual wavefront is shown in Fig. 11(b) with PV = 1.33 μm and RMS = 0.18 μm. As the LCWFC is controlled with open-loop method, the S-H WFS can only measure the correction error of the DM. therefore, the wavefront shown in Fig. 11(b) is the residual after the correction of the DM. According to assumption in section 3.2, after the correction of the first 29 Zernike modes, the residual is 1 rad for the wavelength of 1.2 μm. Thus, the RMS error of residual wavefront is 0.19 μm theoretically. As the RMS error of the corrected wavefront is 0.18 μm, the experimental result is much close to that of the simulation.

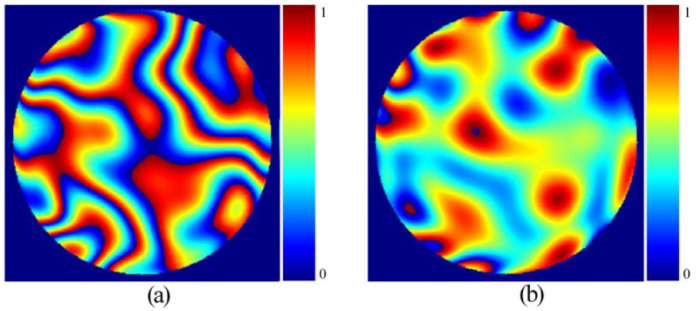

Fig. 11. Wavefront correction with the DM: (a) Before correction; (b) After correction

Optics EXPRESS

To evaluate the effects of the correction, a resolution target (USAF 1951) is chosen as the object. Firstly, the images of the resolution target are shown in Fig. 12 at the waveband of 1.5-1.7 μm without and with adaptive correction. After correction, the fifth element of the fifth group of the USAF target is resolved, with a resolution of 50.8 cycles/mm, thus, the resolution capacity is 19.7 μm. Considering the entrance pupil of the optical system is 20 mm, the diffraction-limited resolution is 19.5 μm for the wavelength of 1.6 μm. Therefore, it can be said that the diffraction-limited resolution is acquired at the waveband of 1.5-1.7 μm with the correction.

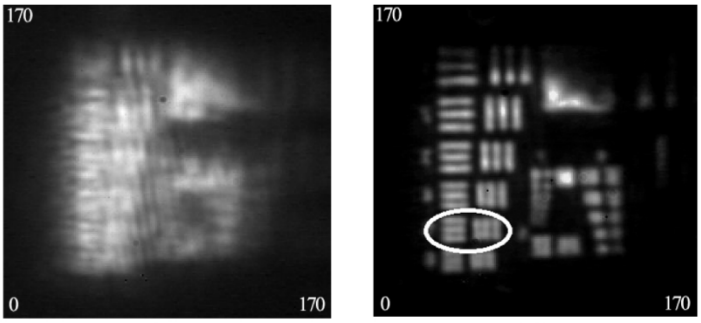

Fig. 12. Images of the USAF target for 1.5-1.7 μm: (a) Without correction; (b) With correction of DM

Similarly, the correction results of the waveband 0.9-1.5 μm can be achieved as shown in Fig. 13. As can be seen, the sixth element of the fifth group was resolved after correction, with the resolution of 57 cycles/mm. Therefore, the resolution capacity is 17.5 μm, which is near the diffraction-limited resolution of 14.6 μm for the wavelength of 1.2 μm.

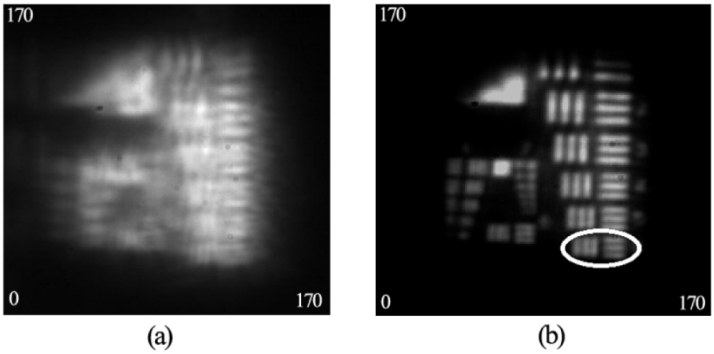

Fig. 13. Images of the USAF target for 0.9-1.5 μm: (a) Without correction; (b) With correction of DM

At last, the images of USAF target are shown in Fig. 14 at the waveband of 0.7-0.9 μm. To do the comparison, the image of the USAF target corrected by the DM is shown in Fig. 14(b). It indicates that, after the correction of the DM, the visible image is still blurry. However, while the aberration with the Zernike modes of 30-77 is corrected, the visible image is resolvable as shown in Fig. 14(c). The fourth element of the sixth group of the target was resolved after correction, with a resolution of 90.5 cycles/mm; thus the resolution capacity is 11 μm. Due to the diffraction limited resolution is 9.76 μm for the wavelength of 0.8 μm, it can be said that a 1.1 times diffraction limited resolution is achieved after the correction.

Optics EXPRESS

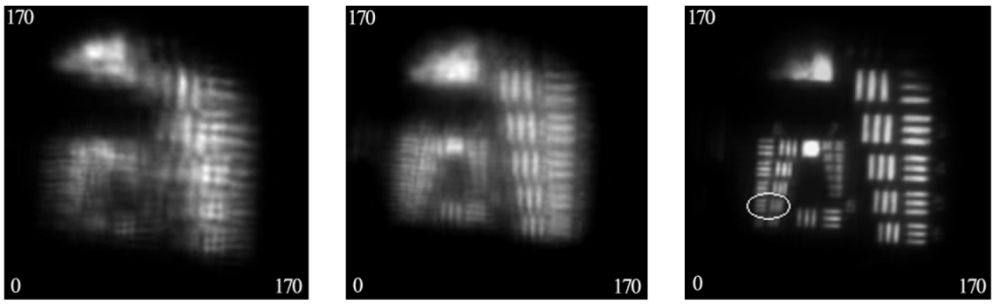

Fig. 14. Images of the resolution target for 700-950nm: (a) Without correction; (b) With correction of DM; (c) With correction of DM and LCWFC.

Based on the above correction results, we can see that the DM/LCWFC AOS can correct the distortions from visible to infrared waveband. After the aberrations corresponding to the first 29 Zernike modes are corrected by the DM, the infrared images are clearly resolved for the wavebands of 0.9-1.5 μm and 1.5-1.7 μm respectively. The clear visible image is also acquired while the higher order aberrations are corrected by the LCWFC. Therefore, the DM/LCWFC combination method is valid and it is very appropriate to be used on larger aperture telescopes to extend the imaging waveband to the visible.

5. Conclusions

In summary, a DM/LCWFC combination AOS is demonstrated to extend the imaging waveband of larger aperture telescopes to the visible. Based on the high spatial resolution of the LCWFC, the high frequency aberrations can be corrected and the clear visible image can be achieved. Hence, the DM is only used to correct the lower frequency aberrations corresponding to the infrared and the demand of the actuators will be decreased greatly. This novel method cannot only avoid the disadvantages of fewer actuators of DM and narrower working waveband of LCWFC, but also utilize the advantages of wide working waveband of DM and high spatial resolution of LCWFC. For example, to a 10 m telescope with r_0 = 10 cm and the imaging wavelength of 0.8 μm, the required actuator number of the DM is 4057. However, to the DM/LCWFC combination system, the actuator number of the DM is reduced to 1538, and the LCWFC only needs 404 × 404 pixels. Hence, the DM/LCWFC AOS can be easily realized compared to the DM based AOS.

The numerical simulation is performed for the DM/LCWFC AOS and a Zernike model method is used to assign the aberration. The simulated results show that, after the first 29 Zernike modes of the aberrations are corrected by DM, the RMS of the residual wavefront is reduced to 0.12 μm and then, it is decreased to 0.03 μm after the 30-77 Zernike modes are corrected by LCWFC. It can be seen that the aberrations can be corrected by the DM/LCWFC system.

At last, an experiment is done to evaluate the validity of the DM/LCWFC AOS. The atmospheric turbulence is produced with an atmospheric turbulence simulator with r_0 = 1 mm (785 nm). The USAF target is used to evaluate the resolution of the optical system. After correction, near diffraction limited resolution USAF target images are obtained at the wavebands of 0.7-0.9 μm, 0.9-1.5 μm and 1.5-1.7 μm respectively. It can be seen that the DM/LCWFC AOS may work at the visible and infrared wavebands for high resolution imaging. Therefore, this novel AOS is a potential method to solve the fabrication bottleneck of the DM and then, the larger aperture telescopes is feasible to work at the visible waveband for high resolution imaging. Further, lots of interesting work may be researched at the visible waveband for the astronomer.

Optics EXPRESS

Funding

Project supported by the National Natural Science Foundation of China (Grant No.61378075, 61405194).

Acknowledgments

This work was supported by State Key Laboratory of Applied Optics, Changchun Institute of Optics, Fine Mechanics and Physics, Chinese Academy of Sciences.